FTIR and dielectric relaxation analysis for PVC-Pb3O4 polymer nanocomposites

T.A. Taha
Jouf University
M.H. Mahmoud
Jouf University
Asif Hayat (asifncp11@yahoo.com)
Fuzhou University https://orcid.org/0000-0003-0949-5305
Ahmad Irfan
King Khalid University

Research Article

Keywords: PVC nanocomposites, Dielectric constant, Energy density, Activation energy

Posted Date: May 10th, 2021

DOI: https://doi.org/10.21203/rs.3.rs-500493/v1

FTIR and dielectric relaxation analysis for PVC-Pb_3O_4 polymer nanocomposites

T.A. Taha[1,2], M.H. Mahmoud[1], Asif Hayat[3], Ahmad Irfan[4],**

[1]Physics Department, College of Science and Arts, Jouf University, P.O. Box 756, Al-Qurayyat, Saudi Arabia

[2]Physics and Engineering Mathematics Department, Faculty of Electronic Engineering, Menoufia University, Menouf 32952, Egypt

[3]State Key Laboratory of Photocatalysis on Energy and Environment, College of Chemistry, Fuzhou University, Fuzhou 350116, China.

[4]Department of Chemistry, Faculty of Science, King Khalid University, Abha 61413, P.O. Box 9004, Saudi Arabia.

Asifncp11@yahoo.com

Abstract

This work studies the FTIR as well as dielectric characteristics of the PVC-Pb_3O_4 nanocomposite films. FTIR analysis shows the small shift in 650, 845 and 1732 cm^{-1} band positions as a confirmation of interaction between Pb_3O_4 nanoparticles with PVC polymer matrix. The real permittivity (ε_1) decreases with increasing frequency for all samples with the appearance of a relaxation peak at high temperatures. The dielectric loss data (ε_2) of the PVC-Pb_3O_4 nanocomposite revealed a shift of the dielectric absorption peak towards high frequency with increasing the temperature. The activation energy values for both α and β relaxations almost decreased with increasing the Pb_3O_4 concentration. The energy density of samples containing Pb_3O_4 has a lower energy density than the pure PVC polymer film. The exponent s often increased with increasing the temperature, and this behavior is consistent with overlapping large-polaron tunneling model. The DC activation energy decreased when the percentage of Pb_3O_4 increased to 3.0 wt% and then increased at 4.0 wt%. Additionally, a convergence between these values and the activation energies of α and β relaxations observed, which is indicates that the same type of charge carriers participate in the processes.

Keywords: PVC nanocomposites; Dielectric constant; Energy density; Activation energy

1. Introduction

Many researchers have recently been interested in studying polymer nanocomposites because of their excellent properties [1, 2]. Studies of polymer nanocomposites grafted with low percentages of fillers have shown distinct properties over conventional composites [3-5]. It appears from the relationship between permittivity and frequency of the polymer that it does not respond immediately upon application of an electric field. The measurement of thermally stimulated depolarization currents used to characterize the segmental mobility and interfacial structures in materials [6]. It is known that inorganic materials possess large permittivity, but suffer from relatively small breakdown strength and mechanical properties due to high sintering temperature and porosity. Although organic polymers possess higher breakdown strength, excellent mechanical properties and handling, they suffer from smaller permittivity [7]. New composite materials were produced through the mixing of inorganic nanoparticles with the polymer matrix and thus developed enhanced dielectric and energy storage properties [8].

One of the distinguished polymers is the polyvinyl chloride (PVC) polymer because of its high performance and low cost. Therefore, PVC is involved in many applications such as pipes, medical devices and insulation cables [9]. Pb_3O_4 ceramic material has a high dielectric constant 13 -17 as reported in the literature [10]. Previous studies investigated the dielectric properties of PVC/inorganic nanoparticle composites. For instance, the addition of Cr_2O_3 nanoparticles to PVC polymer by Hassen et al. led to an increase in the dielectric permittivity and AC conductivity [11]. In El Sayed's work, the dielectric permittivity of PVC was enhanced after adding PbO nanoparticles [12]. Abouhaswa and Taha investigated the dielectric properties of PVC matrix

upon addition of copper oxide nanoparticles [13]. As expected, the dielectric permittivity of PVC nanocomposites improved by addition of nano-CuO particles. Ahmed et al. studied the dielectric properties of graphene nanoplatelet fillers in PVC composites [14]. In their case, dielectric permittivity was also increased by adding the graphene nanoplatelets. Ramazanov and Rahimli investigated dielectric properties of TiO_2 based PVC systems by combining various concentrations of TiO_2 nanoparticles [15]. As depicted, the dielectric permittivity of composites increased at smaller weight fractions but decreased at higher loadings. In contrast, the dielectric constant of PVC polymer films decreased after adding $La_{0.95}Bi_{0.05}FeO_3$ nanoparticles [16].

This work is an extension of our previous research in which we have studied optical and TGA analyses for PVC-Pb_3O_4 polymer nanocomposites [17]. Therefore, we are currently studying the structure of the prepared nanocomposites via FTIR measurements within frequency range (400 – 4000 cm^{-1}). Finally, the broadband dielectric properties of these nanocomposite films were studied at a frequency from 0.1 Hz to 20 MHz at temperatures (303 – 383 K).

2. Experimental details

The polymer nanocomposite films of PVC-Pb_3O_4 with different Pb_3O_4 content prepared by the solution mixing process. In the procedure, 2.0 g PVC powder dissolved in 40 ml THF with stirring for 60 min at 300 K. Then a clear solution obtained and 0.01, 0.03, and 0.04 g of Pb_3O_4 nanoparticles added with stirring for 1h [17]. The polymer nanocomposite solution was poured into a glass dish and dried in the air for 24 h. Finally, polymer films peeled off the glass dish and cut into squares.

JASCO FT/IR-6100 spectrometer was used to measure the FTIR spectra of the PVC-Pb_3O_4 nanocomposite films within the frequency range 400–4000 cm^{-1}. The frequency-dependent dielectric parameters measured using Novocontrol spectrometer within a frequency range from 0.1 Hz - 20 MHz at ambient temperatures from 303 to 383 K with a voltage amplitude of 1 V.

3. Results and discussion

The measured FTIR spectra of PVC-Pb_3O_4 nanocomposite films are displayed in **Fig.1.**

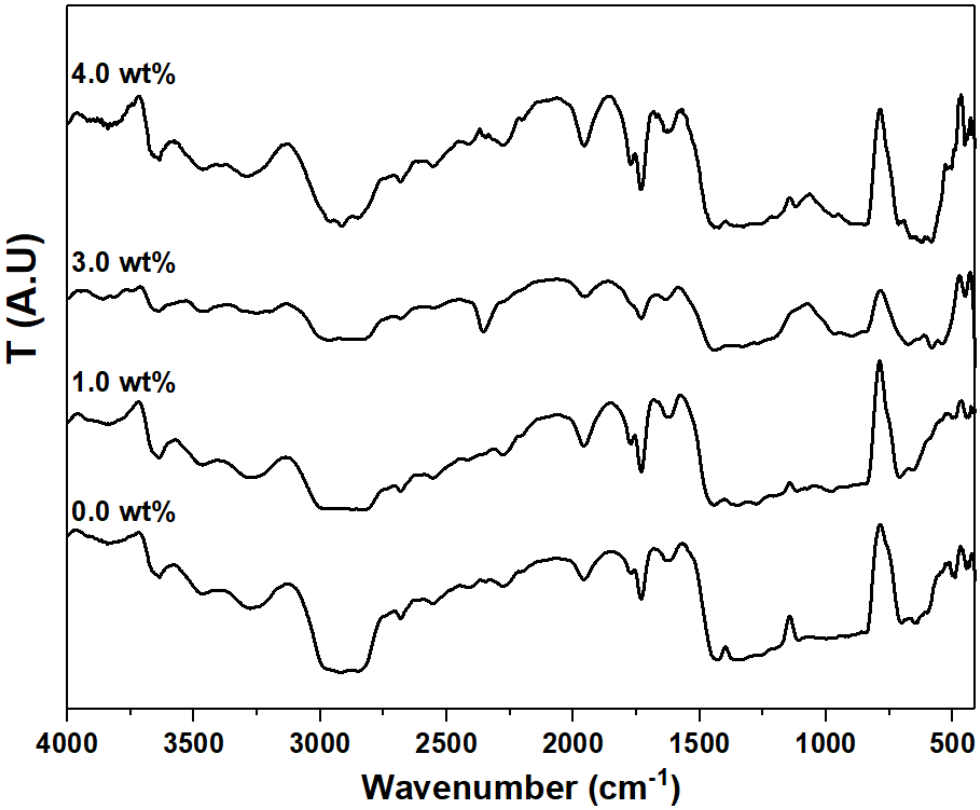

Fig.1. Measured FTIR spectra of PVC films doped with 0, 1, 3 and 4 wt% Pb_3O_4

The absorption bands in the infrared spectrum of polyvinyl chloride at 501, 650 and 700 cm^{-1} are assigned to the amorphous absorption band of C–Cl

stretching, C–Cl crystalline absorption band and isotactic C–Cl stretching, respectively [18]. The band around 845 attributed to υ(C–C) stretching vibrations. The bands at 1110 and 1187 cm^{-1} correspond to perpendicular chain stretch and parallel chain stretch. The absorption band at 1357 cm^{-1} corresponds to CH_2 wag and the other band at 1425 cm^{-1} is due to the bending mode of CH_2. The absorption band at 1624 cm^{-1} is assigned to the carbon-carbon double bond stretching vibration for conjugated bonds, or either aromatic or aliphatic or both. The band at 1732 cm^{-1} is probably from the carbonyl stretching vibration. The wideband at 2915 cm^{-1} corresponds to the CH_2 asymmetric stretching mode, the peak broadening is due to the intermolecular and intra-molecular hydrogen bonds. While the band of OH stretching appeared at 3462 cm^{-1} [19]. For PVC film containing 1.0, 3.0 and 4.0 wt.% of Pb_3O_4 nanoparticles, the same absorption bands are observed. However, the small shift in 650, 845 and 1732 cm^{-1} band positions confirmed the interaction between Pb_3O_4 nanoparticles with PVC polymer matrix.

The complex dielectric constant describe the phenomena of dielectric dispersion through the following relation [20]

$$\boldsymbol{\varepsilon^* = \varepsilon_1 - i\varepsilon_2} \qquad \textbf{(1)}$$

where ε_1 is the real permittivity and imaginary part ε_2 is known as dielectric loss. Frequency dependence real dielectric permittivity (ε_1) for PVC-Pb_3O4 nanocomposite films at various temperatures presented in **Fig.2**. It is obvious that the higher the temperature, the better the dielectric constant of all the films.

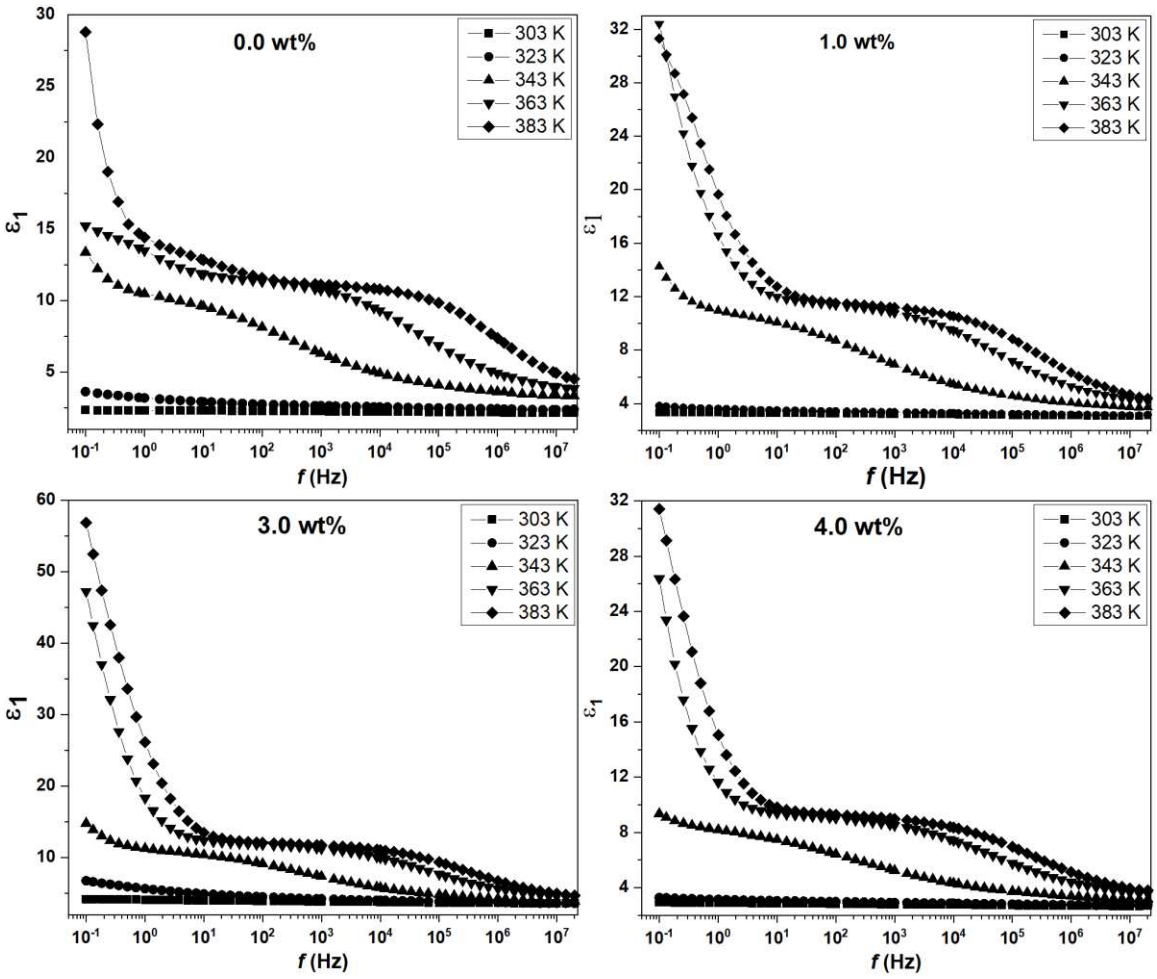

Fig.2. Measured real dielectric permittivity at different temperatures for the PVC-Pb_3O_4 films

Fig.2 shows the effect of increasing the permittivity due to an increase in temperature from 303 to 383 K. We also noticed from the figure that the real permittivity decreases with increasing frequency for all samples with the appearance of a relaxation peak at high temperatures. The decrease in real permittivity with increasing the frequency is explained by the decrease of space charge polarization. As the space charge polarization increased at a lower frequency, a potential barrier was generated and the charges accumulated at the grain boundary to increase the real permittivity [20].

The dielectric loss data (ε_2 vs. f) of the PVC-Pb_3O_4 nanocomposites **(Fig.3)** indicates that the dielectric loss values are observed to be increasing more rapidly at low frequency. On further inspection of **Fig.3**, one may notice a shift of the dielectric absorption peak towards high frequency with increasing the temperature. The Arrhenius activation model is the simplest one that is applied to describe the temperature dependence of relaxation times through the condition $\omega_{max}\tau = 1$. Thus the Arrhenius temperature behavior of relaxation frequency given by [21]:

$$f_{max} = f_o e^{\left(\frac{-E_a}{k_\beta T}\right)} \qquad (2)$$

where f_o is constant, E_a the activation energy and k_β Boltzmann's constant From the plots of $\ln(f_{max})$ vs. 1000/T, which are linear, values for the apparent activation energies are derived **(Fig.4)**.

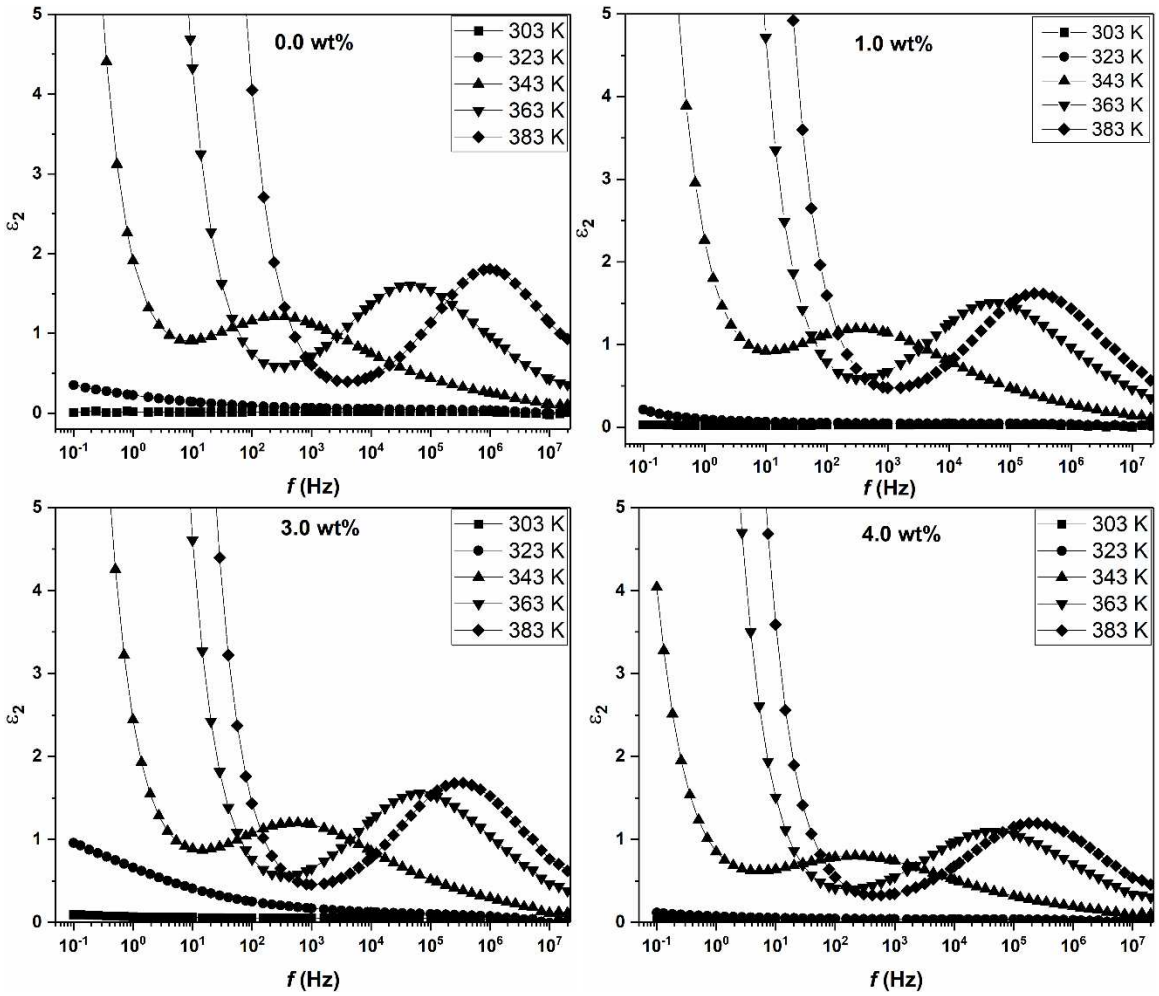

Fig.3. Plot of ε_2 vs. frequency for PVC-Pb_3O_4 nanocomposite films

In **Table.1** the values of the activation energy for β and α relaxations were recorded for the different nanocomposite films. In general, the activation energy values for both α and β relaxations decreased with increasing the Pb_3O_4 concentration.

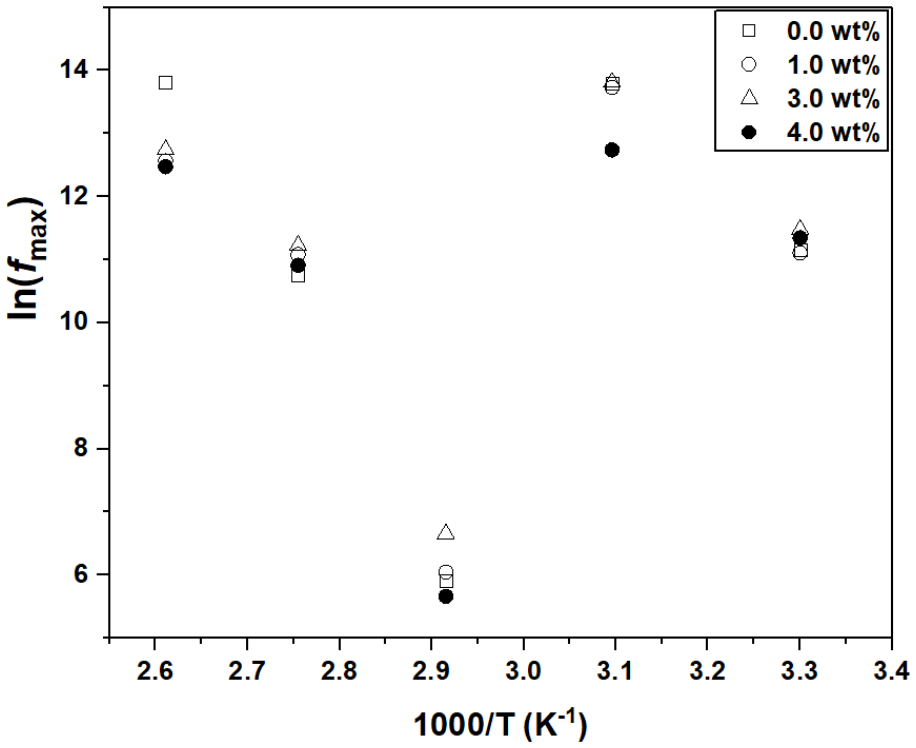

Fig.4. Plots of ln(f_{max}) versus 1000/T for the PVC-Pb_3O_4 nanocomposite films

Table.1. Activation energies of the PVC--Pb_3O_4 nanocomposite films

Pb_3O_4 content	**E_a (eV)**	
	β	**α**
0.0 wt%	1.11	2.25
1.0 wt%	1.10	1.86
3.0 wt%	0.98	1.74
4.0 wt%	0.59	1.94

In polymer composites, the main relaxation α-transition is related to the glass transition of the polymer and refers to cooperative transitions and the relaxation β-transition closest to the glass transition temperature associate this transition with the motions of short (smaller than a segment) sections of the

main chain, the mobility of the side groups and their fragments. In connection with this, as the ratio of Pb_3O_4 increased in the PVC polymer matrix, the activation energies for rotational and translational movements of segments and cooperative modes of segmental mobility decrease. One can estimate the corresponding gain in energy density (electrostatic energy) for a linear dielectric through the following relationship [22];

$$\boldsymbol{U = \frac{1}{2}\varepsilon_0\varepsilon_1 E^2} \qquad \textbf{(3)}$$

where U is the maximum energy density the dielectric can contain, ε_0 is the permittivity of free space, ε_1 is the relative permittivity of the dielectric and E is the electric field is proportional to the voltage applied (E = V/d). In **Fig.5a**, the energy density is estimated at 303 K as a function of Pb_3O_4 content. Samples containing Pb_3O_4 have a lower energy density than the pure PVC polymer film. This result could be due to the decrease of real permittivity (ε_1) and increased dielectric loss (ε_2). As the temperature increase, the energy density increase for all nanocomposite films **(Fig.5b)**. This increase in the energy density is due to the high mobility of large polymer chains and interfacial polarization [23].

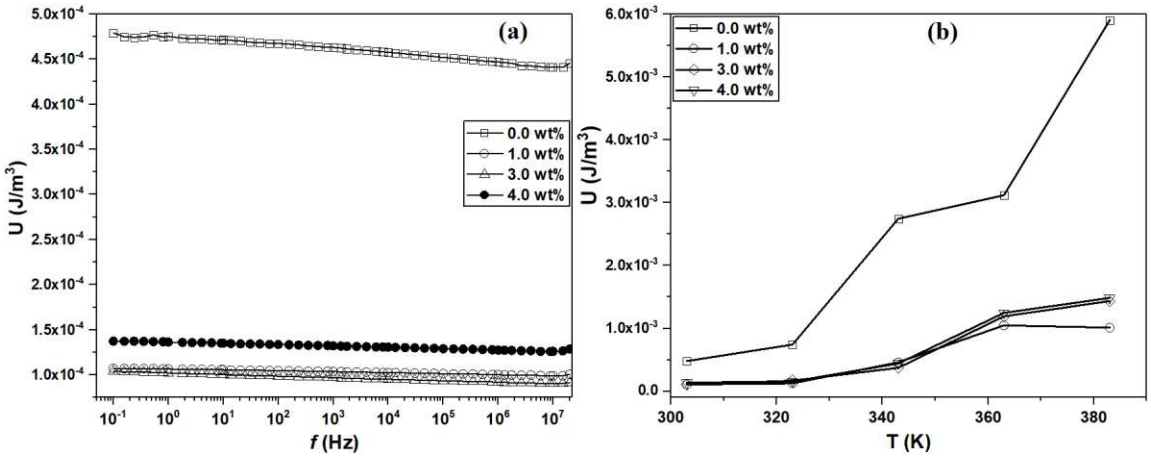

Fig.5. Variation of energy density (U) with (a) frequency at 303 K and (b) temperature at 0.1 Hz for all nanocomposite films

The electric modulus analysis can describe relaxation phenomena in different materials. The expression for the electric modulus (M^*) is given by [24];

$$\boldsymbol{M^* = \frac{1}{\varepsilon^*} = \frac{1}{\varepsilon_1 - j\varepsilon_2} = \frac{\varepsilon_1}{\varepsilon_1^2+\varepsilon_2^2} + j\frac{\varepsilon_2}{\varepsilon_1^2+\varepsilon_2^2} = M_1 + jM_2} \qquad \textbf{(4)}$$

Where M_1 defines the real electric modulus and M_2 is the imaginary part electric modulus. We can see in **Fig.6** that at low frequencies, the values of M_1 are lowered as the temperature rises in all nanocomposite films. This comes due to reducing the contribution of electrode polarization [25]. We also notice an increase in M_1 with increasing frequency at all temperatures.

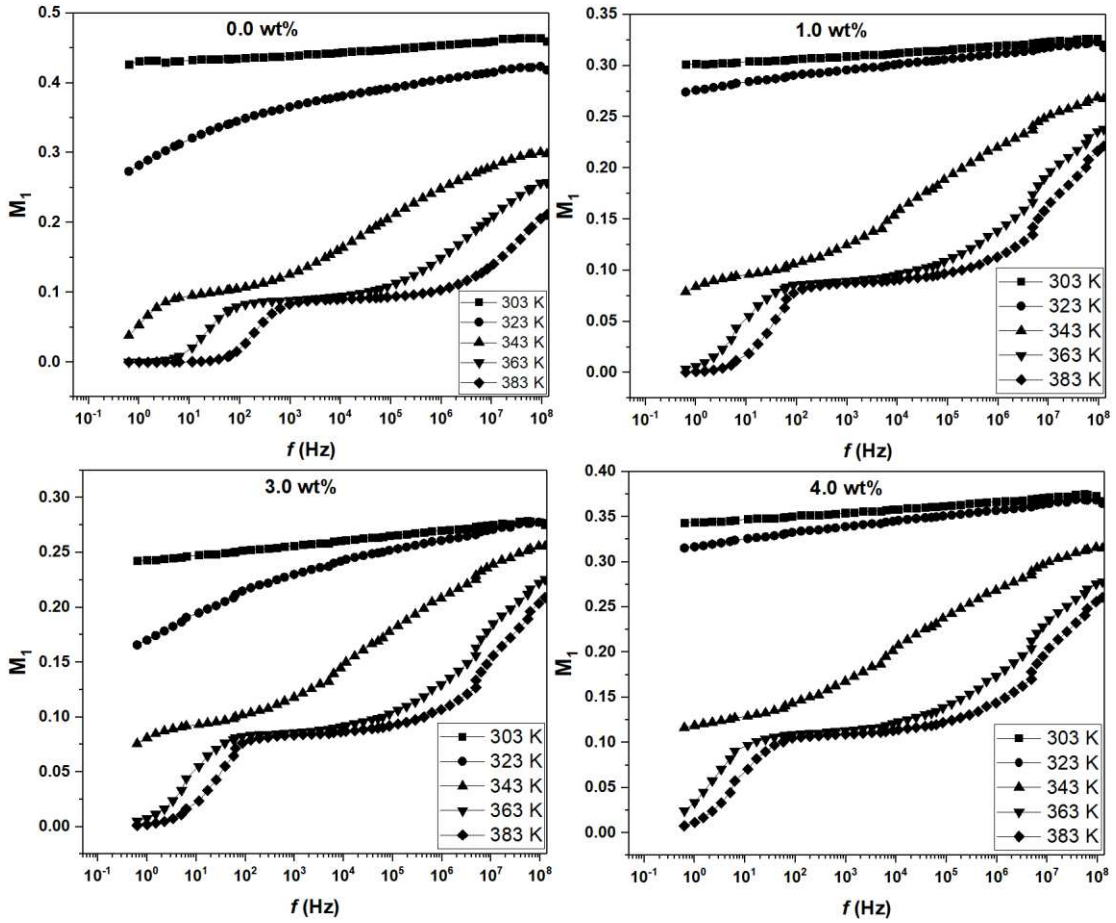

Fig.6. Plots of M_1 versus frequency at different temperatures for the PVC-Pb_3O_4 nanocomposite films

The imaginary part of electric modulus (M_2) for the PVC--Pb_3O_4 nanocomposite films presented in **Fig.7**. At low frequency, the electrode polarization is suppressed with increasing the temperature. At high temperatures, two relaxation processes are depicted and shifted to the high-frequency side.

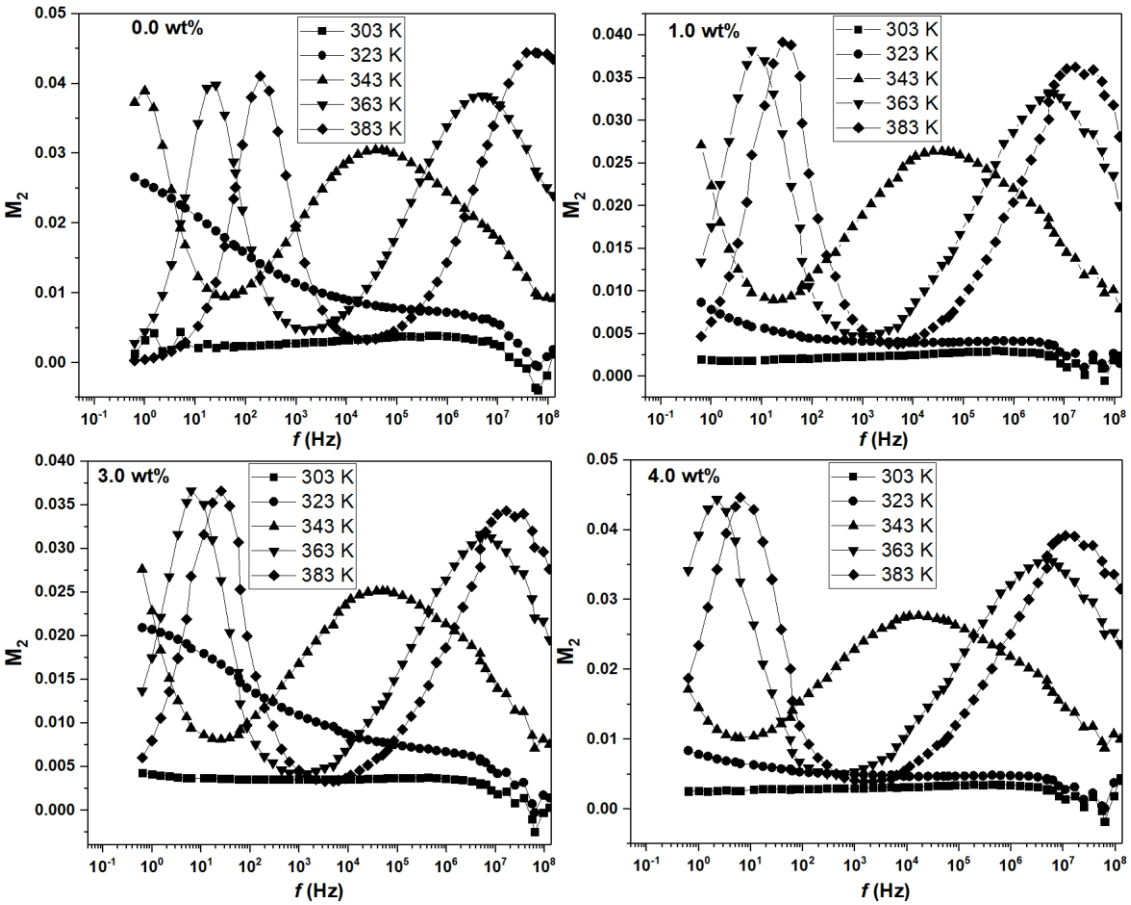

Fig.7. Graphs of M_2 versus frequency at different temperatures for the PVC-Pb_3O_4 nanocomposite films

Additionally, the imaginary electric modulus (M_2) related to the frequency (ω) by the modified Kohlrausch-Williams-Watts (KWW) relation [26]:

$$M_2 = \frac{M_2^{max}}{(1+\beta)+\frac{\beta}{1+\beta}\left[\beta\left(\frac{\omega_{max}}{\omega}\right)+\left(\frac{\omega}{\omega_{max}}\right)^{\beta}\right]} \qquad (5)$$

Where M_2^{max} denotes the maximum value of M_2 at ω_{max} and β is the KWW parameter. After fitting the graphs in **Fig.7** with **eq.5**, the values of β are evaluated and recorded in **Table.2**.

Table.2. The evaluated β values for the PVC--Pb_3O_4 nanocomposite films

Pb_3O_4 percentage	**303 K**	**323 K**	**343 K**	**463 K**	**483 K**
0.0 wt%	0.62	0.55	0.31	0.45	0.32
1.0 wt%	0.46	0.50	0.26	0.43	0.57
3.0 wt%	0.59	0.50	0.26	0.41	0.57
4.0 wt%	0.59	0.50	0.24	0.40	0.50

As shown in **Table.2**, the estimated values of β less than 1.0, which correlated with non-Debye relaxation [27],

The frequency-dependent conductivity spectra described previously by the following Jonscher power law [28],

$$\sigma_{AC} = \sigma_{DC} + A\omega^{s} \quad (6)$$

Where A and s are temperature-dependent parameters. This procedure allows analyzing directly the temperature–activated behavior of conduction. Such analysis is useful to reveal the nature of charge species participating in conduction, where the exponent s lies between $0 < s < 1$.

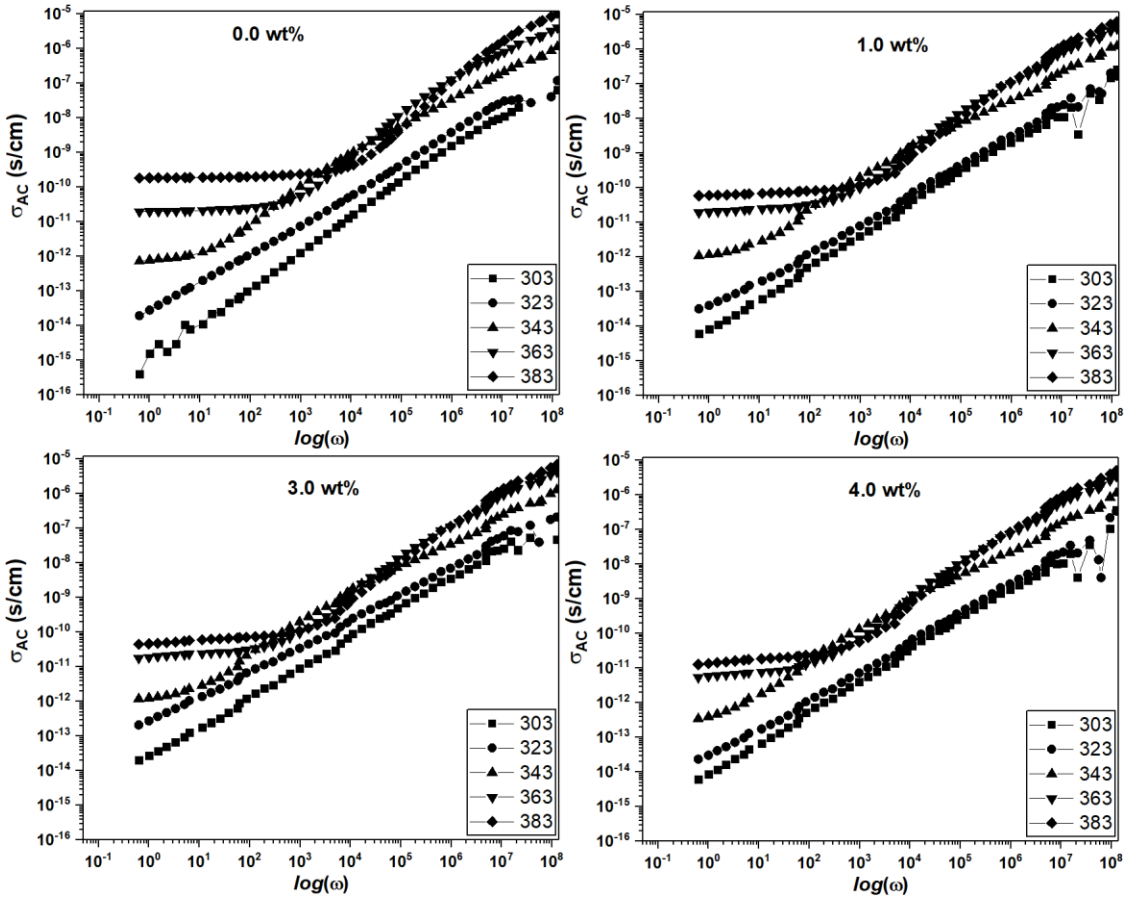

Fig.8. Plots of σ_{AC} versus frequency at different temperatures for the PVC-Pb_3O_4 nanocomposite films

Table.3. The estimated values of s for PVC--Pb_3O_4 nanocomposite films

	Pb_3O_4 percentage	**303 K**	**323 K**	**343 K**	**463 K**	**483 K**
	0.0 wt%	0.99	0.90	0.76	0.75	0.99
	1.0 wt%	0.82	0.84	0.73	0.83	0.98
	3.0 wt%	0.78	0.81	0.76	0.88	0.99
	4.0 wt%	0.81	0.87	0.82	0.85	0.92

The values of exponent s are evaluated after fitting the experimental data with **eq.6**. As shown in **Table.3**, the exponents often increased with increasing the

temperature, and this behavior is consistent with overlapping large-polaron tunneling model [29].

The DC conductivity σ_{DC} of a given sample is calculated as the plateau value of (f) at low frequency (0.1 Hz) in **Fig.8**. For further analysis, the extrapolated values of σ_{DC} usually plotted as a function of temperature as an Arrhenius plot **(Fig.9)**, which is the plot of the ln(σ_{DC}) as a function of the inverse temperature (1000/T). The Arrhenius temperature behavior of conductivity is given by [30]:

$$\boldsymbol{\sigma_{DC} = Be^{\frac{-E_a}{k_\beta T}}} \qquad \textbf{(7)}$$

Here E_a is the temperature-independent activation energy, k_β is the Boltzmann's constant, B is the pre-exponential factor.

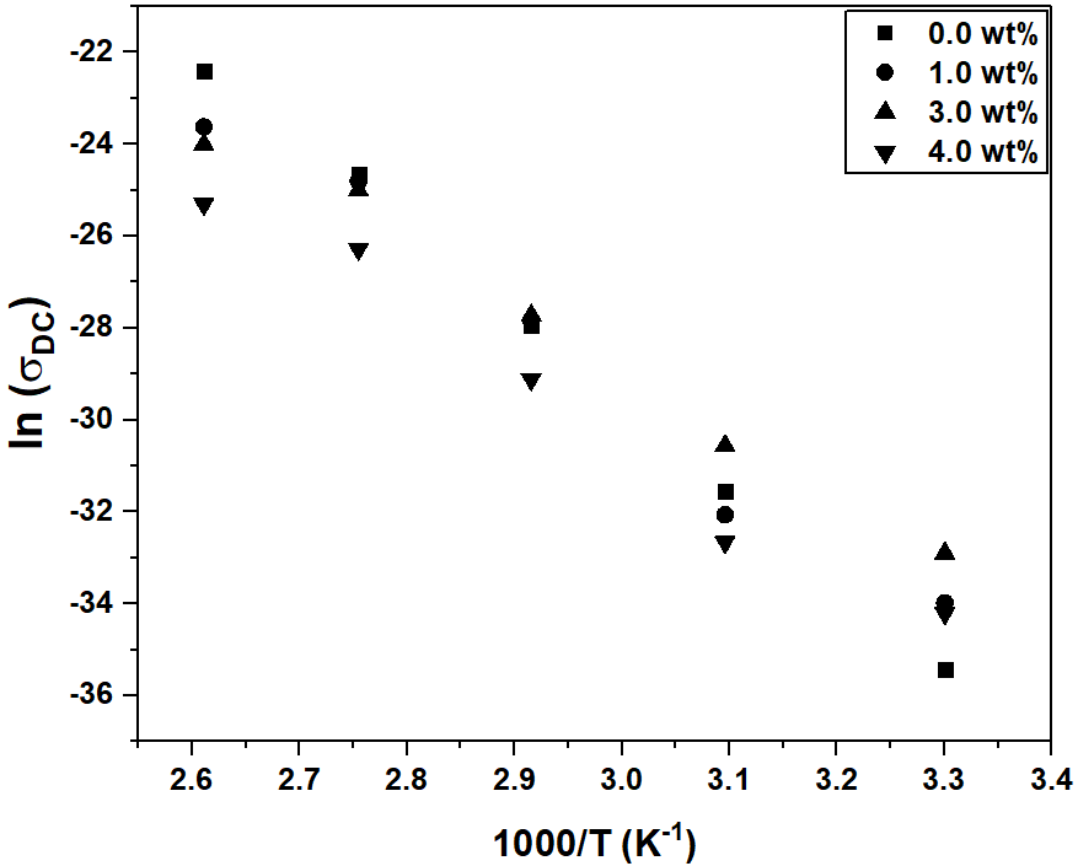

Fig.9. Graphs of ln(σ_{DC}) as a function of the inverse temperature (1000/T) for the PVC-Pb_3O_4 nanocomposite films

The values of activation energy obtained from the slope of the straight lines in **Fig.8** using the **eq.7**. Hence, the values were 1.65, 1.40, 1.17 and 1.21 eV for the nanocomposite films at 0.0, 1.0, 3.0 and 4.0 wt% Pb_3O_4. We notice a convergence between these values and the activation energies of α and β relaxations, which is an indication that the same type of charge carriers participate in the processes [27]. The DC activation energy also decreased when the percentage of Pb_3O_4 increased to 3.0 wt% and then increased at 4.0 wt%.

4. Conclusion

This research deals with a study of the structure as well as dielectric properties of the PVC-Pb_3O_4 nanocomposite films. FTIR analysis showed a small shift in 650, 845 and 1732 cm^{-1} band positions as a confirmation of interaction between Pb_3O_4 nanoparticles with PVC polymer matrix. Dielectric measurements show that the real dielectric constant (ε_1) decreased with increasing frequency for all samples with the appearance of a relaxation peak at high temperatures. Plots of the dielectric loss (ε_2) for the PVC-Pb_3O_4 nanocomposites revealed a shift of the dielectric absorption peak towards high frequency with increasing the temperature. The activation energies for both α and β relaxations almost decreased with increasing the Pb_3O_4 concentration. The energy density of samples containing Pb_3O_4 has a lower energy density than the pure PVC polymer film. The exponent s often increased with increasing the temperature, and this behavior is consistent with overlapping large-polaron tunneling model. The DC activation energy decreased when the

percentage of Pb_3O_4 increased to 3.0 wt% and then increased at 4.0 wt%. Additionally, a convergence between these values and the activation energies of α and β relaxations observed, which is indicates that the same type of charge carriers participate in the processes.

5. Acknowledgments

1- The authors extend their appreciation to the Deputyship for Research & Innovation, Ministry of Education in Saudi Arabia for funding this work through the grant number (375213500).

2- The authors would like to extend their sincere appreciation to the central laboratory at Jouf University for support this study.

6. References

1. Guo, M., et al., High-Energy-Density Ferroelectric Polymer Nanocomposites for Capacitive Energy Storage: Enhanced Breakdown Strength and Improved Discharge Efficiency. Materials Today, 2019. **29**.
2. Donya, H., et al., Micro-structure and optical spectroscopy of PVA/iron oxide polymer nanocomposites. Journal of Materials Research and Technology, 2020. **9**(4): p. 9189-9194.
3. Taha, T.A., Z. Ismail, and M.M. Elhawary, Structural, optical and thermal characterization of PVC/SnO_2 nanocomposites. Applied Physics A, 2018. **124:307**(4): p. 307.
4. Taha, T.A., M.H. Mahmoud, and H.H. Hamdeh, Development, thermal and dielectric investigations of PVDF-Y_2O_3 polymer nanocomposite films. Journal of Polymer Research, 2021. **28**(5).

5. Taha, T.A. and M.A.A. Alzara, Synthesis, thermal and dielectric performance of PVA-$SrTiO_3$ polymer nanocomposites. Journal of Molecular Structure, 2021(4): p. 130401.
6. Kuliev, M.M., R.S. Ismaiilova, and M.N. Bairamov, Study of polymer composites by methods of thermoactivated spectroscopy. Surface Engineering & Applied Electrochemistry, 2008. **44**(6): p. 467-470.
7. YANG, et al., Dependence of dielectric properties on BT particle size in EP/BT composites. , 2006(z2): p. 250-250.
8. Hemida, T. and A. Saleh, Dynamic mechanical and optical characterization of PVC/fGO polymer nanocomposites. Applied Physics A, 2018. **124**(9).
9. Tata, B., et al., Fluorescence and dielectric spectroscopy identification of polyvinyl chloride/NiO nanocomposites. Journal of Molecular Structure. **1212**.
10. Terpstra, H.J., R. Groot, and C. Haas, The electronic structure of the mixed valence compound Pb_3O_4. The journal of physics and chemistry of solids, 1997. **58**(4): p. p.561-566.
11. Sayed, A.E., et al., Synthesis, characterization, optical, and dielectric properties of polyvinyl chloride/cadmium oxide nanocomposite films. Polymer Composites, 2014. **35**(9): p. 1842–1851.
12. Sayed, A. and W.M. Morsi, Dielectric relaxation and optical properties of polyvinyl chloride/lead monoxide nanocomposites. Polymer Composites, 2013. **34**(12).
13. Abouhaswa, A. and T. Hemida, Tailoring the optical and dielectric properties of PVC/CuO nanocomposites. Polymer Bulletin, 2019(7).
14. Ahmed, R.M., et al., Structural, mechanical, and dielectric properties of polyvinylchloride/graphene nano platelets composites. International

Journal of Polymer Analysis and Characterization, 2021. **26**(1): p. 68-83.

15. Ramazanov, M.A. and A.M. Rahimli, The Study of the Morphology and Dielectric Properties of PVC+TiO_2-Based Nanocomposites. Integrated Ferroelectrics, 2019.
16. Taha, T.A. and A.A. Azab, Thermal, optical, and dielectric investigations of PVC/La0.95Bi0.05FeO_3 nanocomposites. Journal of Molecular Structure, 2018. **1178**.
17. T., A., and Taha, Optical and thermogravimetric analysis of Pb_3O_4/PVC nanocomposites. Journal of Materials Science: Materials in Electronics, 2017.
18. Gerrard, D.L. and W.F. Maddams, The Resonance Raman Spectrum of Degraded Poly(vinyl chloride). 2. γ-Irradiated Samples. Macromolecules, 1977. **10**(6): p. 1221-1224.
19. Silva, D., et al., Aceitação de diferentes itens alimentares por machos e fêmeas jovens de muçuãs (Kinosternon scorpioides) em cativeiro.
20. Taha, T.A., S. Elrabaie, and M.T. Attia, Exploring the Structural, Thermal and Dielectric Properties of PVA/Ni0.5Zn0.5Fe_2O_4 Composites. Journal of Electronic Materials, 2019. **48**(7).
21. Yang, L., et al., Novel polymer ferroelectric behavior via crystal isomorphism and the nanoconfinement effect. Polymer, 2013. **54**(7): p. 1709-1728.
22. Mohamed, et al., Nanocomposites Based on Chitosan-Graft-Poly(N-Vinyl-2-Pyrrolidone): Synthesis, Characterization, and Biological Activity. International Journal of Polymeric Materials and Polymeric Biomaterials, 2015. **64**(11).

23. Sanida, A., et al., Development, characterization, energy storage and interface dielectric properties in $SrFe_{12}O_{19}$/epoxy nanocomposites. Polymer, 2017: p. S0032386117305189.
24. A, E.F., O.W.G. A, and E.A. B, A.C. conductivity and relaxation dynamics in zinc–borate glasses. Progress in Natural Science: Materials International, 2012. **22**(2): p. 86-93.
25. Ahm, A., B. Oga, and C. Srs, Effect of very fine nanoparticle and temperature on the electric and dielectric properties of MC-PbS polymer nanocomposite films - ScienceDirect. Results in Physics. **16**.
26. Tarasov, V.E., Chapter 16 Fractional Temporal Electrodynamics. 2011.
27. Thakur, V., et al., Temperature dependent electrical transport characteristics of $BaTiO_3$ modified lithium borate glasses. AIP Advances, 2015. **5**(8): p. 87110-87110.
28. Dhahri, A., E. Dhahri, and E.K. Hlil, Electrical conductivity and dielectric behaviour of nanocrystalline $La_{0.6}Gd_{0.1}Sr_{0.3}Mn_{0.75}Si_{0.25}O_3$. Rsc Advances, 2018. **8**.
29. Karmakar, S., et al., Dielectric relaxation behavior and overlapping large polaron tunneling conduction mechanism in NiO–PbO μ-cauliflower composites. Journal of Alloys and Compounds, 2020. **851**: p. 156789.
30. Donya, H. and T.A. Taha, Preparation, structure and optical properties of ZnTe and PbTe nanocrystals grown in fluorophosphate glass. Journal of Materials Science Materials in Electronics, 2018. **29**(10): p. 1-7.

Figures

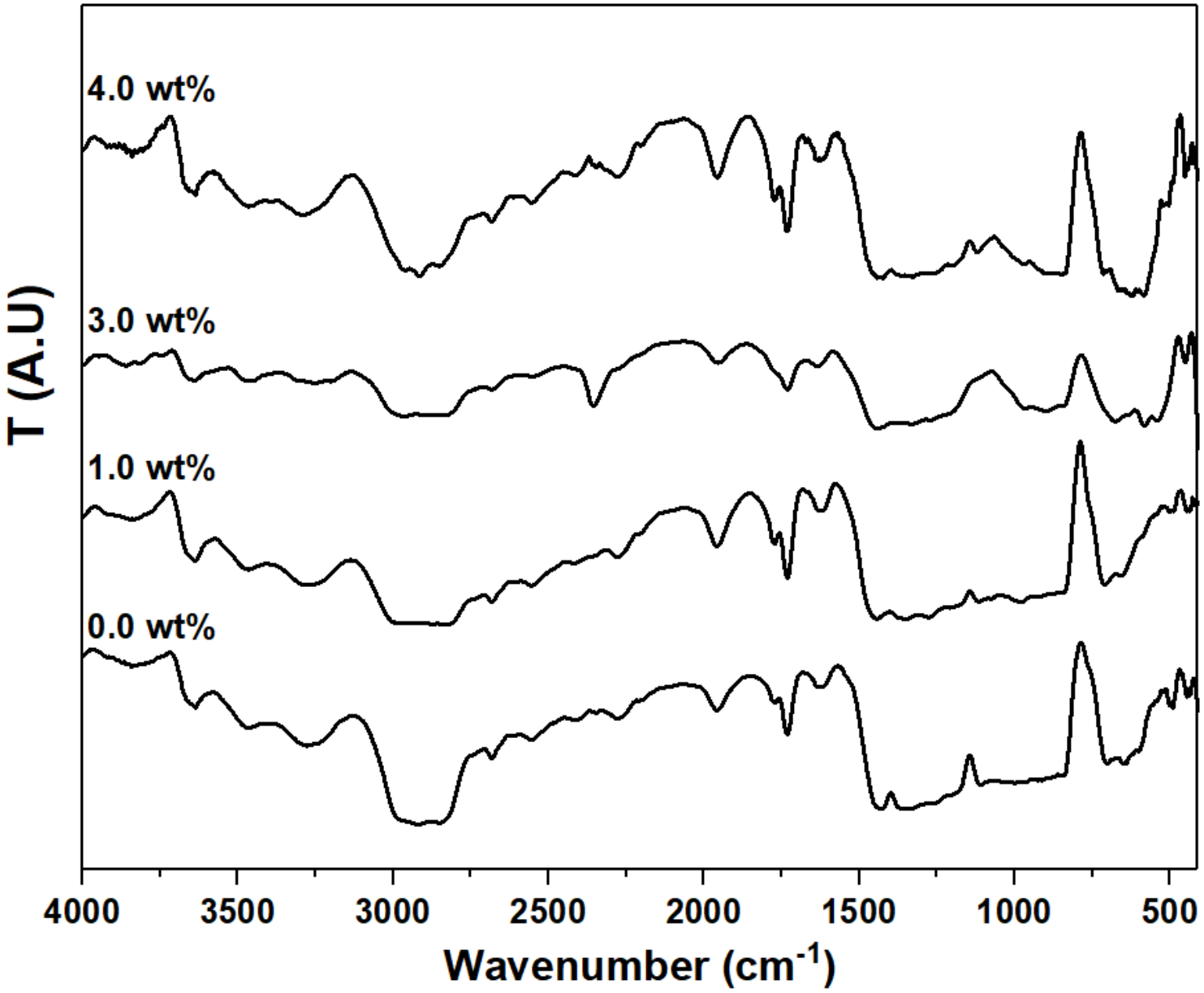

Figure 1

Measured FTIR spectra of PVC films doped with 0, 1, 3 and 4 wt% Pb3O4

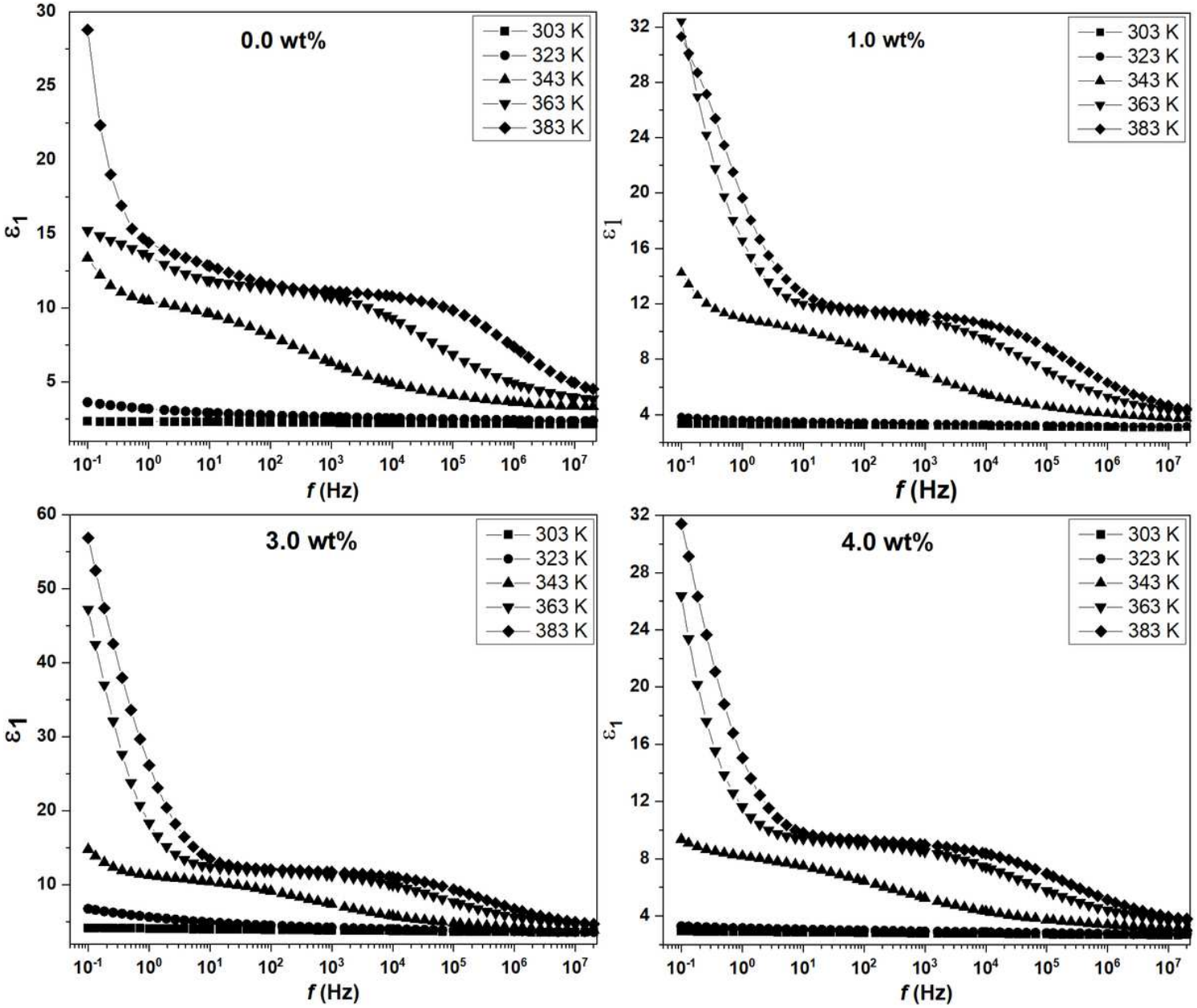

Figure 2

Measured real dielectric permittivity at different temperatures for the PVC-Pb3O4 films

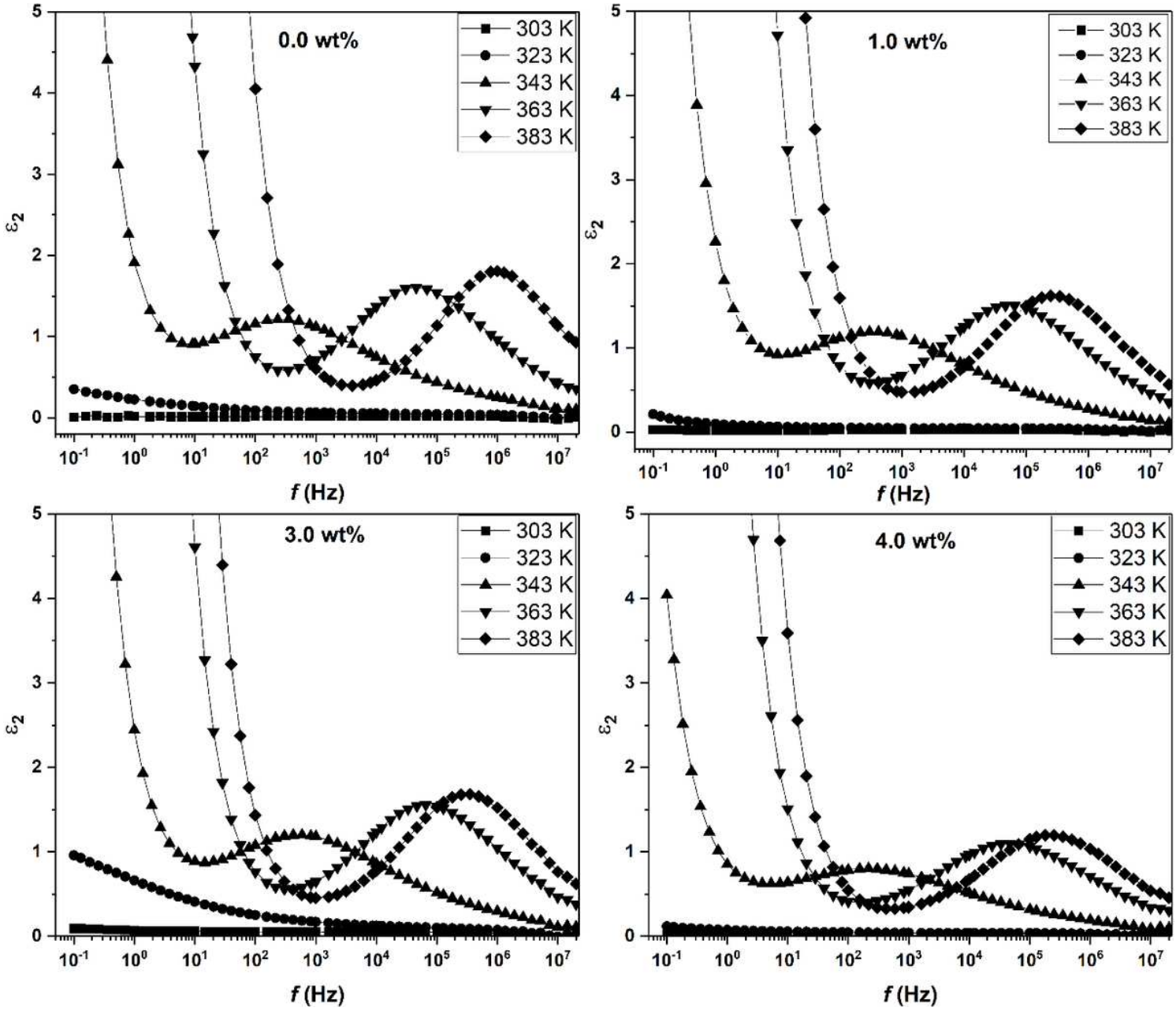

Figure 3

Plot of ε2 vs. frequency for PVC-Pb3O4 nanocomposite films

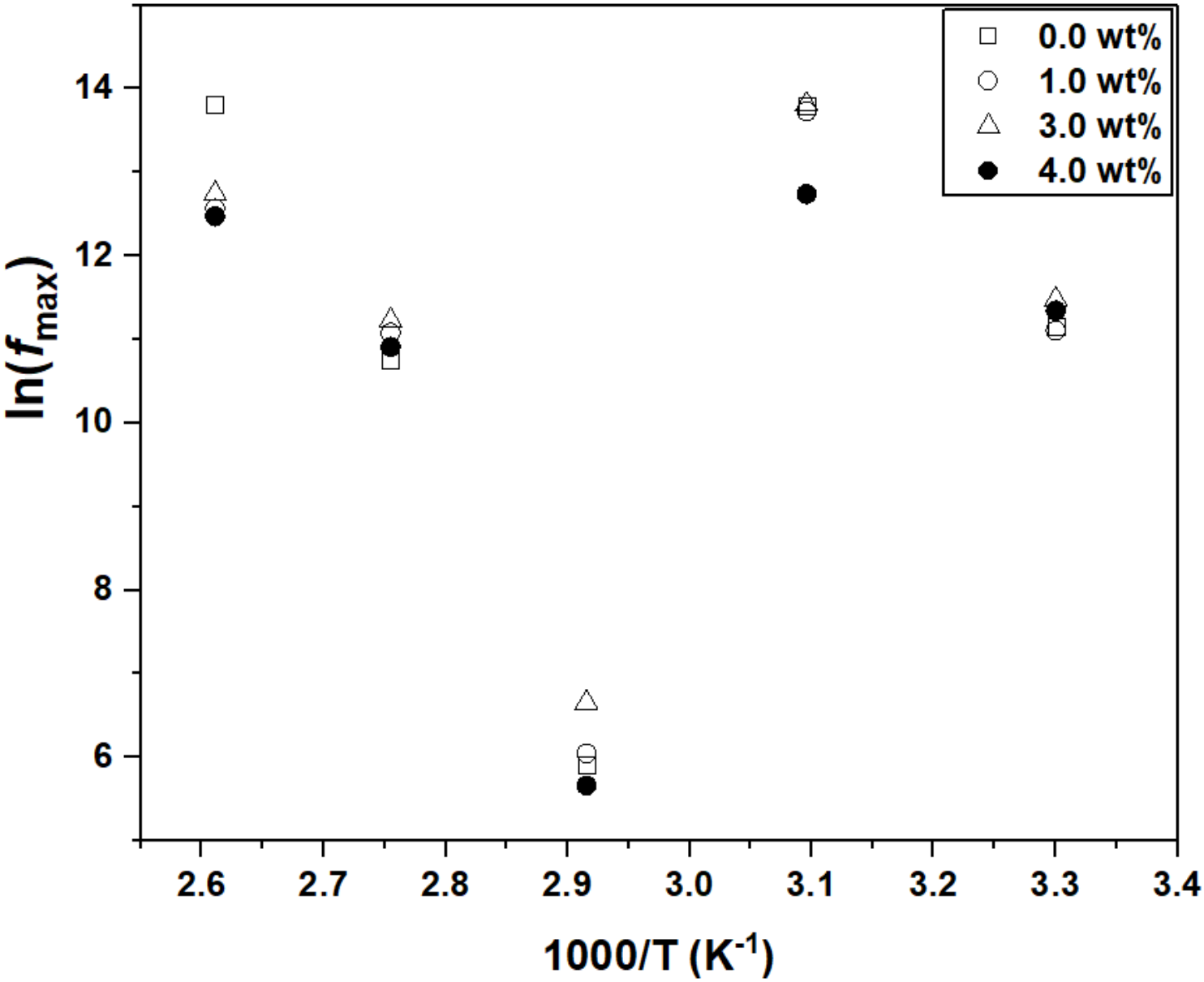

Figure 4

Plots of ln(fmax) versus 1000/T for the PVC-Pb3O4 nanocomposite films

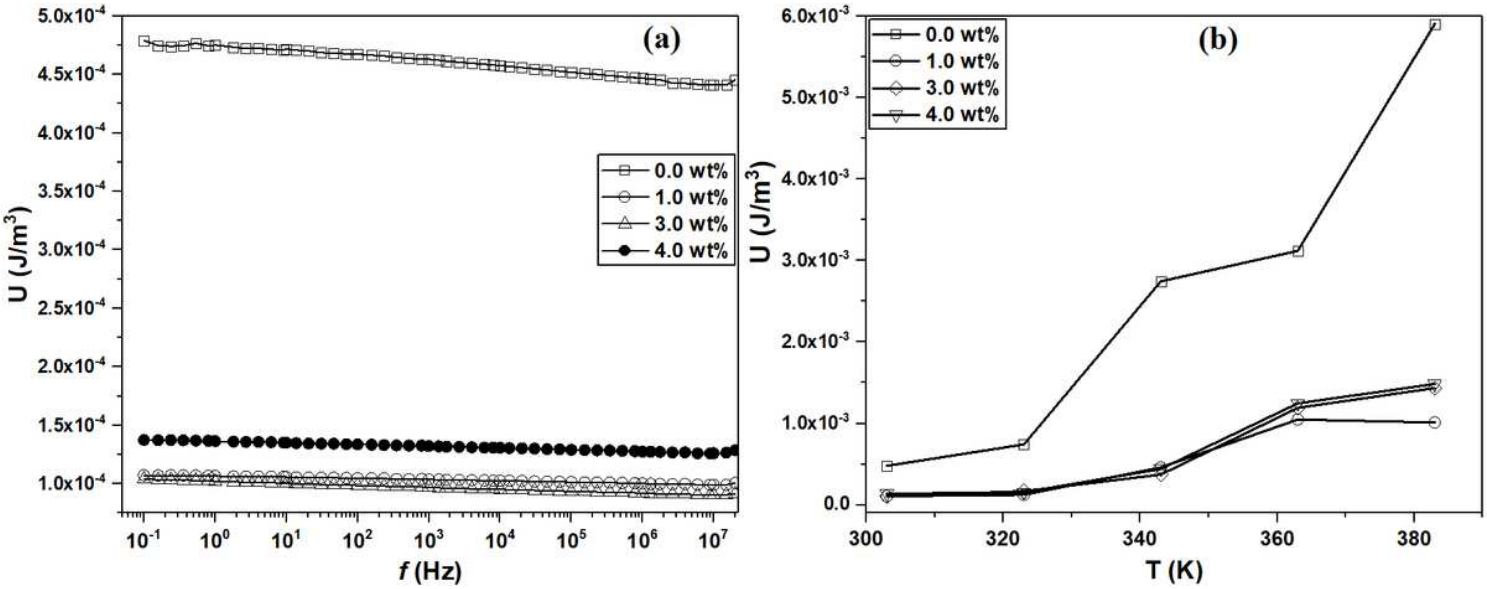

Figure 5

Variation of energy density (U) with (a) frequency at 303 K and (b) temperature at 0.1 Hz for all nanocomposite films

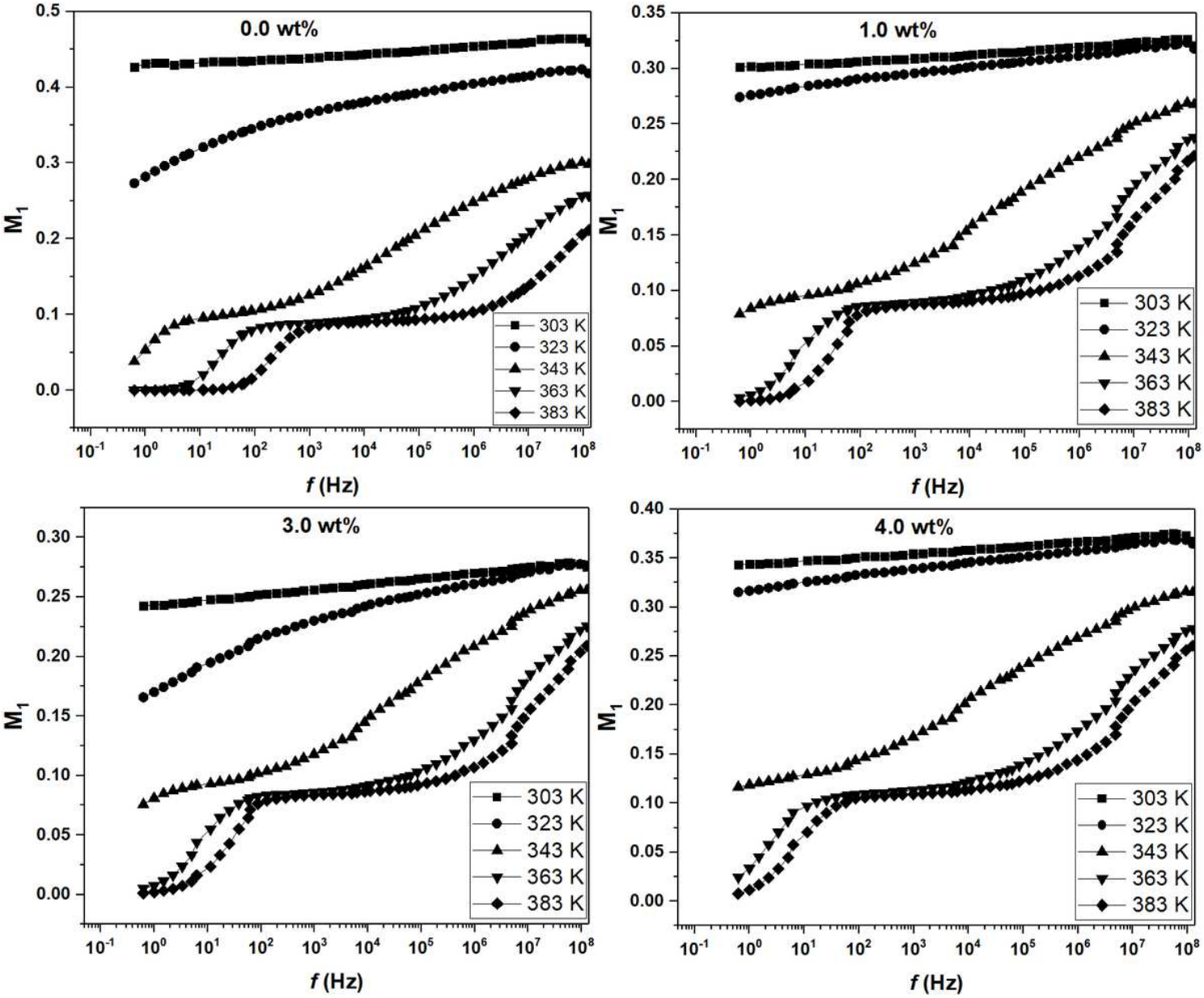

Figure 6

Plots of M1 versus frequency at different temperatures for the PVC-Pb3O4 nanocomposite films

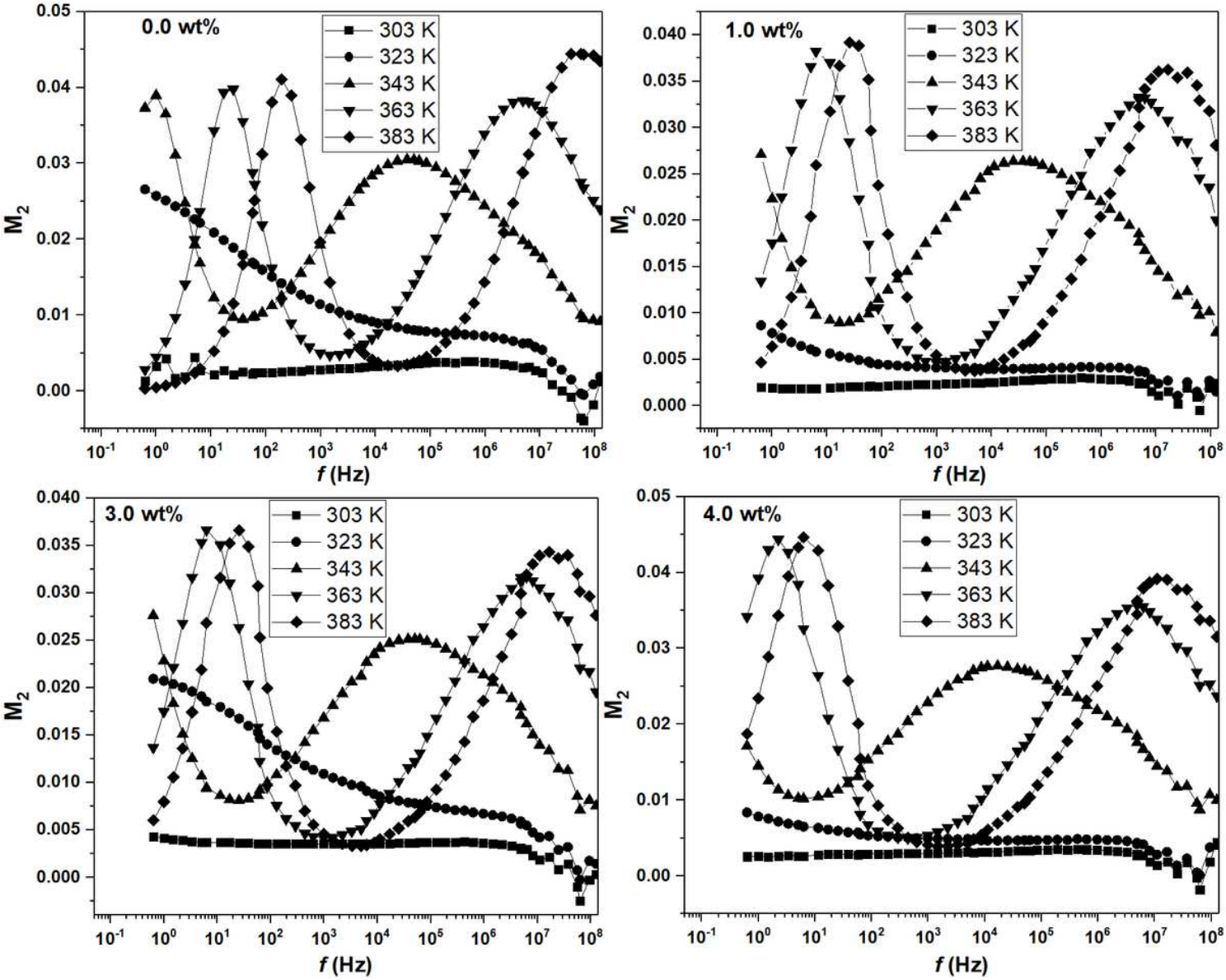

Figure 7

Graphs of M2 versus frequency at different temperatures for the PVC-Pb3O4 nanocomposite films

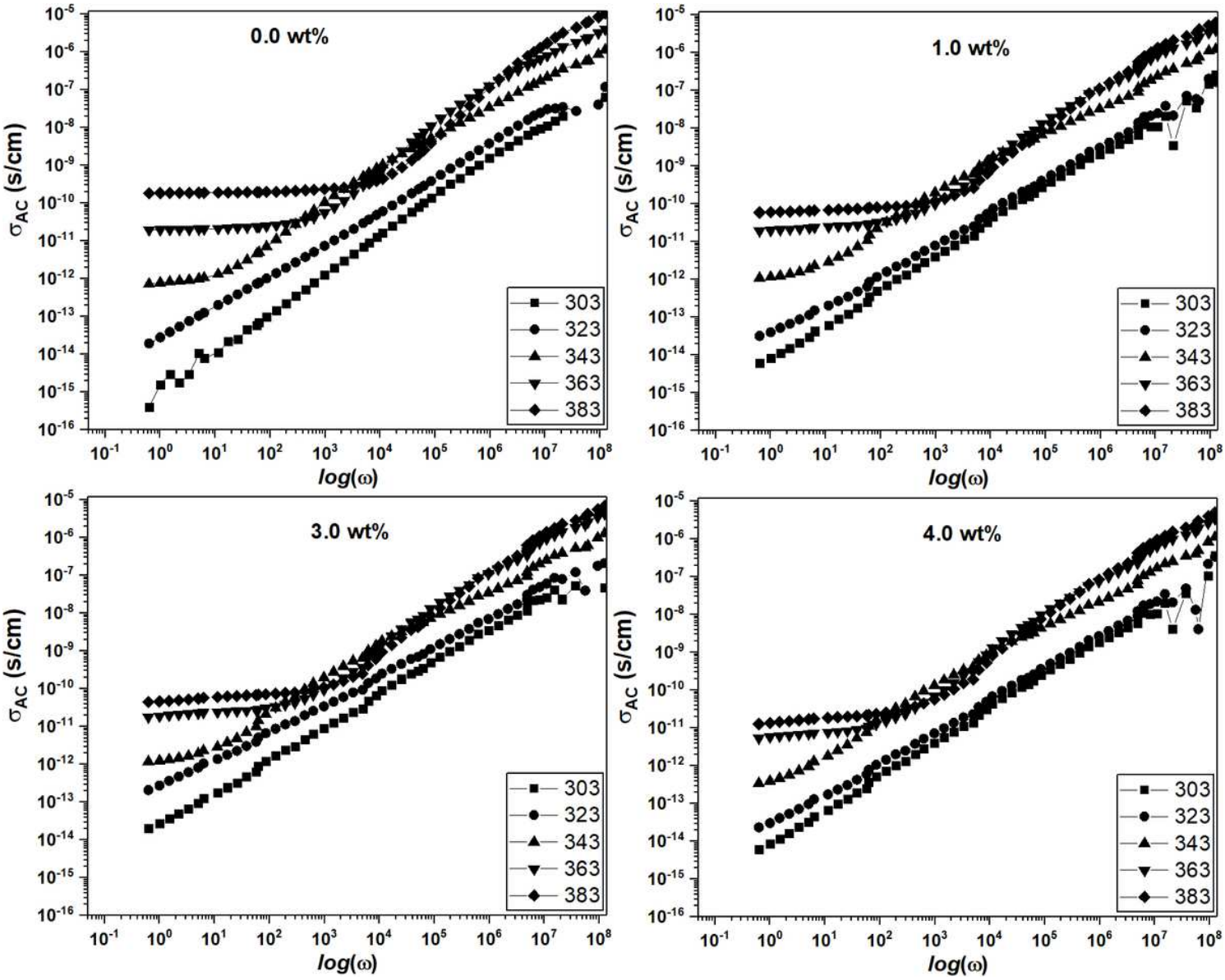

Figure 8

Plots of σAC versus frequency at different temperatures for the PVC-Pb3O4 nanocomposite films

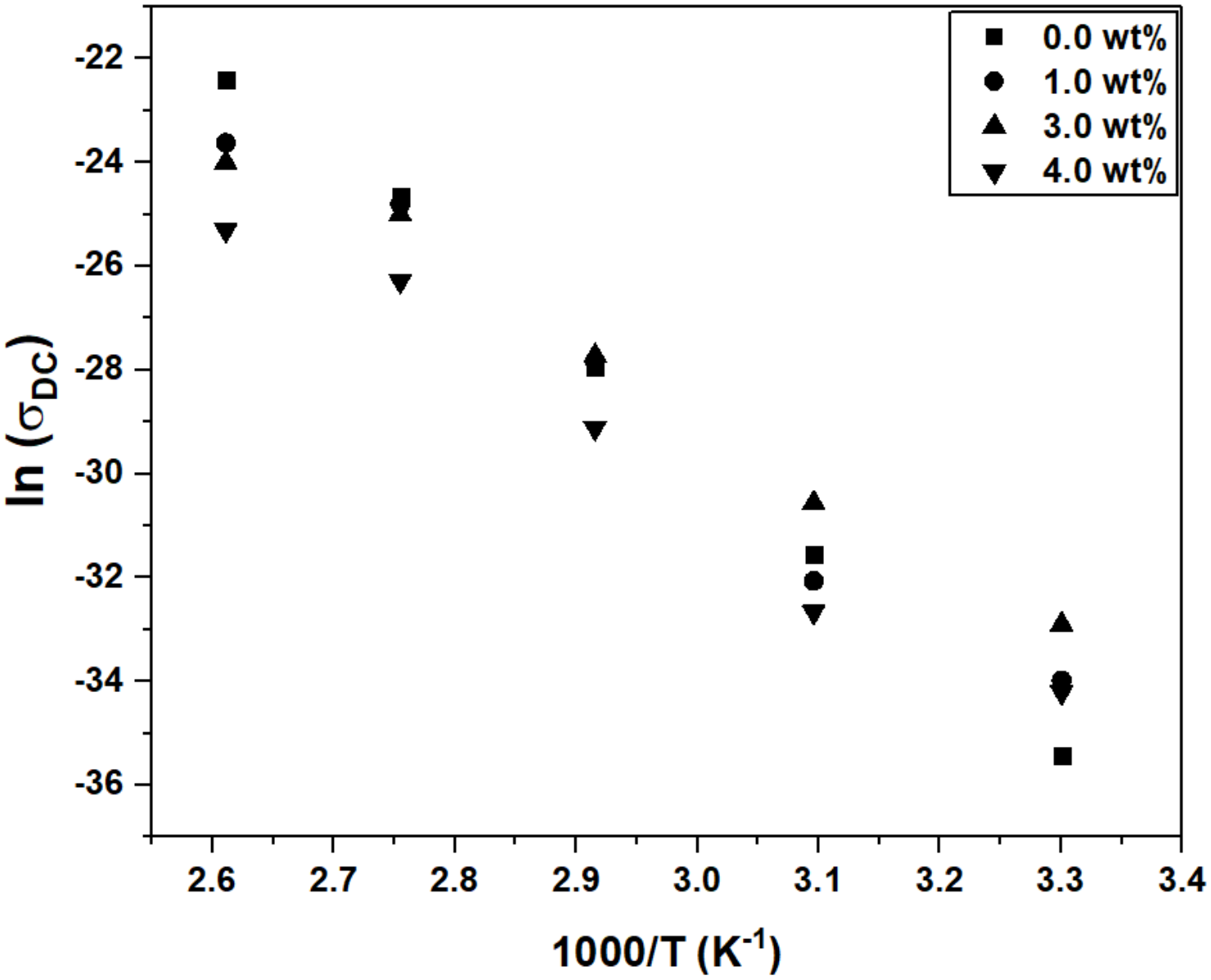

Figure 9

Graphs of ln(DC) as a function of the inverse temperature (1000/T) for the PVC-Pb3O4 nanocomposite films

Supplementary Files

This is a list of supplementary files associated with this preprint. Click to download.

- Highlights.docx